Electronic Supplementary Material (ESI) for Journal of Materials Chemistry A.

Supporting Information

Oxygen Vacancies on the Surface of H_xWO_{3-y} for Enhanced Charge Storage

Haiyan Wang, Ruxue Fan, Jingyu Miao, Jiayi Chen, Shanjun Mao, Jiang Deng, Yong Wang*

Advanced Materials and Catalysis Group, Institute of Catalysis, Zhejiang University, Hangzhou 310028, PR China

Methods

Preparation of H_xWO_{3-y}/NCC and WO_3/NCC. A piece of carbon cloth (CC, HCCP330, Shanghai Hesen Electric Co. Ltd., China) was cleaned with ethanol, water and dried before use. CC was then annealed at 1000 ^oC in industry N_2 with a heating rate of 5 ^oC min^{-1} to obtain porous CC[1], which was served as the flexible conductive carbon substrate for loading of tungsten oxide. 1 g ammonlum metatungstate ($(NH_4)_6H_2W_{12}O_{40}\cdot XH_2O$, Aladdin) was dissolved in 20 mL deionized water adequately and porous CC was immersed in the solution for 1 h. Then, it was taken out and dried at 70 ^oC in an oven. Finally, porous CC loaded with ammonlum metatungstate was annealed in high purity N_2 (99.99% purity) at 700 ^oC for 1 h with a rate of 2 ^oC min^{-1} to synthesize H_xWO_{3-y}, denoted as H_xWO_{3-y}/NCC. WO_3/NCC was synthesized according to the same procedure to the H_xWO_{3-y}/NCC, except replacing the annealing atmosphere with industry nitrogen (99% purity). The mass density for H_xWO_{3-y} (WO_3) is about 2 mg cm^{-2}.

Preparation of e-H_xWO_{3-y}/NCC. Ar^+ plasma etching process was carried out to remove the surface OVs layer of H_xWO_{3-y}. Specifically, the synthesized H_xWO_{3-y}/NCC was etched with Ar^+ ions for 30 s at 3 keV and the final product was collected and denoted as e-H_xWO_{3-y}/NCC.

Preparation of NCC. Similar to H_xWO_{3-y}/NCC and WO_3/NCC, CC was first annealed at 1000 ^oC in industry N_2 with a heating rate of 5 ^oC min^{-1} to obtain porous CC. Then the obtained porous CC continue to anneal at 700 ^oC in high purity N_2 or industry N_2 with a heating rate of 5 ^oC min^{-1} to obtain NCC. Note that NCC obtained no matter in high purity N_2 or industry N_2 both show similar specific surface area (825 m^2 g^{-1} vs. 896 m^2 g^{-1}, Fig. S2a and Table S1) and similar electrochemical performance (CV curve, Fig. S2b). Therefore, they both were denoted as NCC without special distinction.

Characterization. Scanning electron microscopy (SEM) was conducted using Zeiss Sigma field emission SEM (Model 8100). High-resolution transmission electron microscopy (HRTEM) characterization was carried out with Tecnai G2 F30 S-Twin at an acceleration voltage of 300 KV. Raman spectrometer (JY, HR 800) with an 514 nm Ar laser excitation source was employed to obtain Raman spectra. X-ray photoelectron spectra (XPS) were taken with an ESCALAB MARK II spherical analyzer using an aluminum anode (Al 1486.6 eV). A Nicolet Fourier transform infrared spectroscopy was used to record FT-IR spectra. X-ray diffraction (XRD) data was collected with a D/tex-Ultima TV wide angle X-ray diffractometer equipped with Cu Kα radiation (λ=1.54 Å). N_2 adsorption-desorption analysis was measured with micromeritics ASAP 2020 HD88 at 77 K. The specific surface area (SSA) and pore size distribution (PSD) were recorded based on Brunauere-Emmette-Teller (BET) method and density functional theory (DFT) pore model, restively.

Electrochemical measurements. Electrochemical measurements were carried out in a three-electrode cell with a Gamry Reference 600 electrochemical workstation. Platinum sheet and saturated calomel electrode (SCE) electrodes were used as the counter and reference electrodes, respectively and 5 M LiCl as the electrolyte solution. Two-electrode configuration was conducted with 5 M LiCl as the electrolyte to estimate the feasibility of H_xWO_{3-y}/NCC for energy storage. Freestanding H_xWO_{3-y}/NCC was directly used as electrode materials without the need of current collectors and any other conductive additives.

OVs generation mechanism

According to the results, it is found that H_XWO_{3-y} can only be produced in a pure N_2, while in industry N_2 (99.99% purity), WO_3 is produced. These indicate that a pure oxygen depleted condition is important for synthesis of OVs in H_XWO_{3-y}. Additionally, ammonlum metatungstate as raw materials can also produce reduced gases. What's more, it is found that NCC is important to produce OVs in H_XWO_{3-y}/NCC, as only WO_3 with yellow color is produced when the same procedure was conducted without the intrusion of NCC (Figure S22). This phenomenon may because NCC with functional groups can produce various reduced gases during pyrolysis at high temperature, and the in-situ synthesis process may promise carbon substrate as reducing agent to reduce W^{6+} to W^{5+}, and generate OVs simultaneously. Therefore, the OVs generation mechanism can be concluded as the following formula:

$$2W^{6+} + O^{2-} + H_2 \xrightarrow{C} 2W^{5+} + V_O + H_2O$$

Where O^{2-} is lattice oxygen and V_O is oxygen vacancy.

In the synthesis process, when hydrogen intercalation in the octahedra structure of WO_3, it will produce H_xWO_{3-y}.

Charge Storage Mechanism

The adsorption/desorption (at surface) or intercalation/de-intercalation (at subsurface) of cations involved in the charge storage process of WO_3 can be described as the following formula:

$$WO_3 + x\,Li^+ + x\,e^- \leftrightarrow Li_x\,WO_3$$

Based on the ex situ XPS results (Figure 3), the charging and discharging of WO_3 only involves the transition between W^{6+} and W^{5+}. However, the introduction of OVs in H_xWO_{3-y} could draw the electrons to the reaction sites. In the reaction sites, more oxygen vacancies and more reduced W ions will improve the redox reaction activities of H_xWO_{3-y}. Thus, during the charging and discharging, more reduced W^{5+} and W^{4+} was produced, improving their charge storage properties.

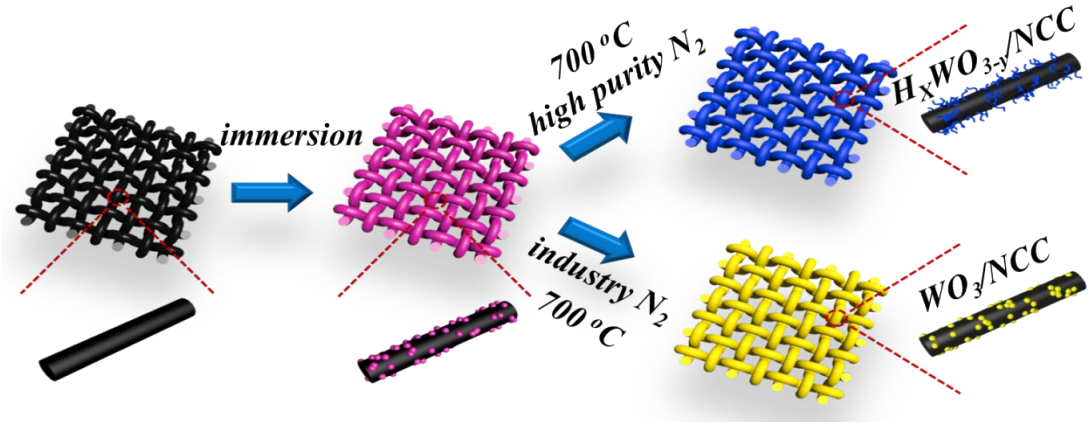

Fig. S1 Schematic representation of the fabrication process for H_xWO_{3-y}/NCC and WO_3/NCC.

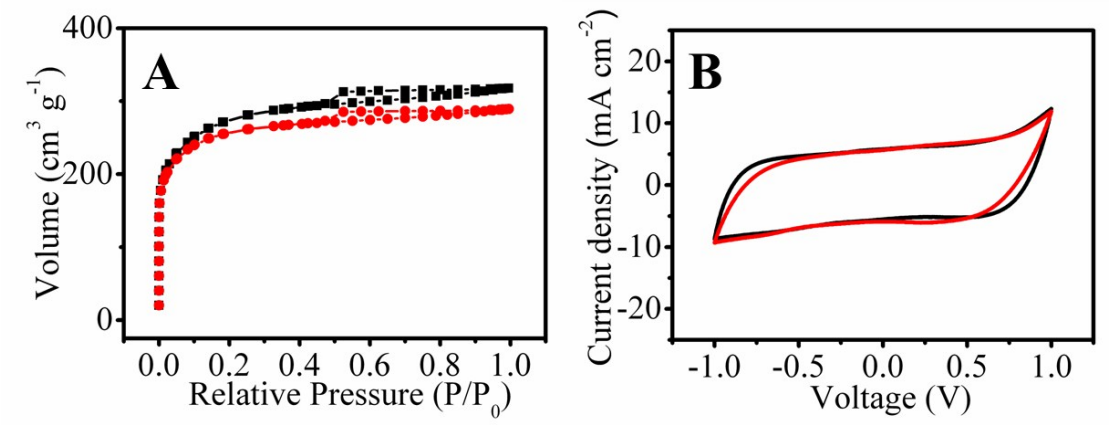

Fig. S2 (A) N_2 adsorption-desorption curves and (B) CV curves at 5 mV/s for NCC annealed according to the procedures for H_xWO_{3-y}/ NCC (red curves) and WO_3/NCC (blue curves).

Table S1 Porosity measurements NCC annealed according to the procedures for H_xWO_{3-y}/ NCC (red curves) and WO_3/NCC (blue curves) in Figure S2 using nitrogen adsorption/desorption tests.

Materials	S_{BET}[a] ($m^2\ g^{-1}$)	Pore volume ($cm^3\ g^{-1}$)			Average pore width (nm)
		V_{Total}[b]	V_{Micro}[c]	V_{Micro}/V_{Total}	
NCC in H_xWO_{3-y}/ NCC	825	0.45	0.39	0.87	2.16
NCC in WO_3/NCC	895	0.49	0.41	0.84	2.19
[a] Brunuaer–Emmett–Teller surface area; [b] Calculated by single-point adsorption; [c] Calculated by t-plot method.					

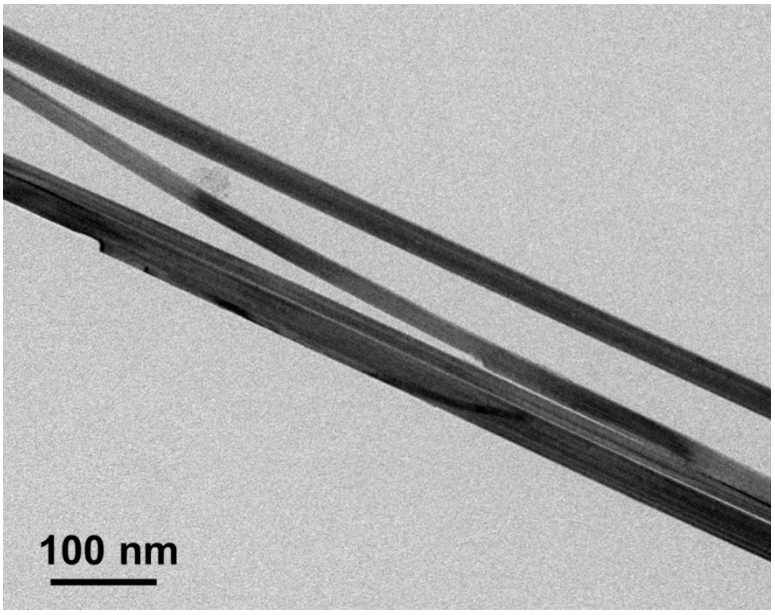

Fig. S3 TEM image of H_xWO_{3-y} nanowires.

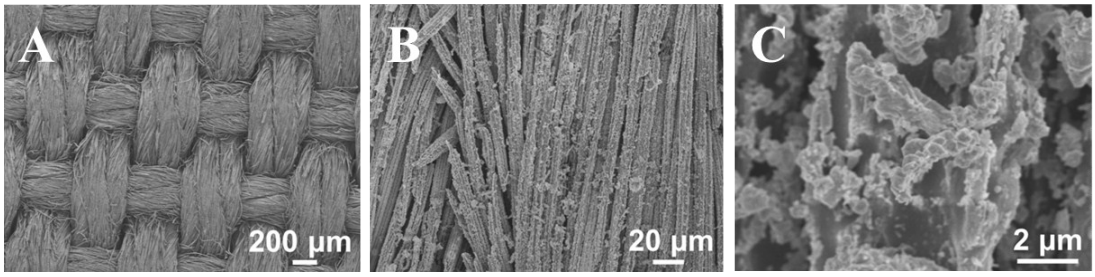

Fig. S4 SEM images of WO_3/NCC.

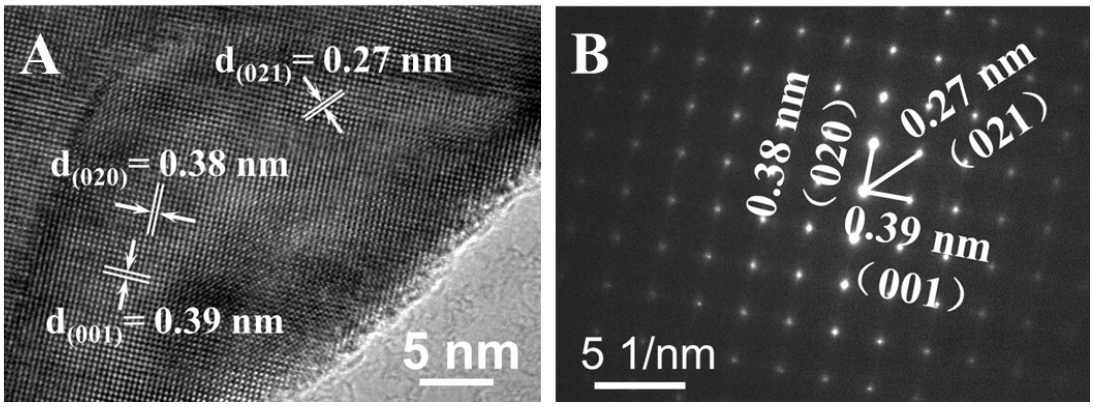

Fig. S5 (A) HRTEM imageof WO_3. (B) SAED pattern of WO_3.

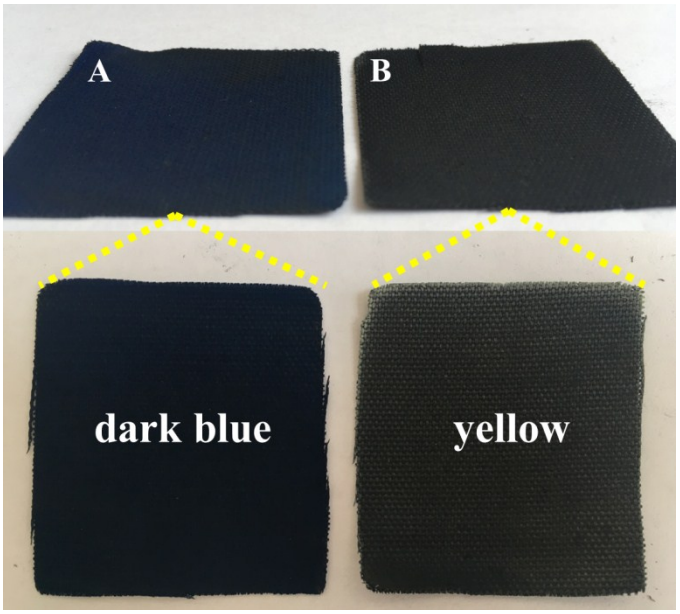

Fig. S6 The digital graph for (A) H_xWO_{3-y}/NCC and (B) WO_3/NCC, showing the color for (A) H_xWO_{3-y} is dark blue and (B) for WO_3 is yellow.

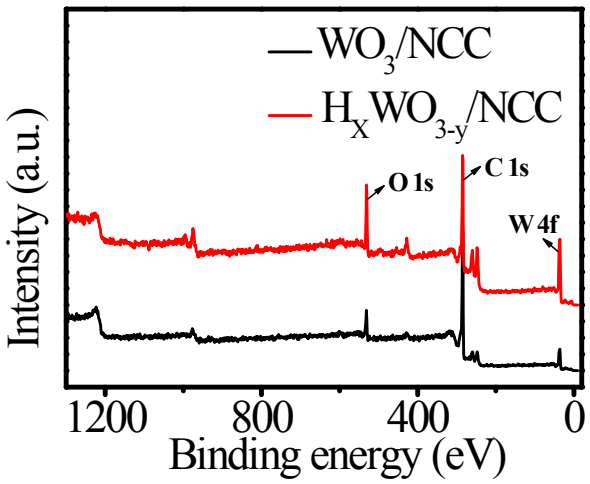

Fig. S7 XPS spectra of H_xWO_{3-y}/NCC and WO_3/NCC.

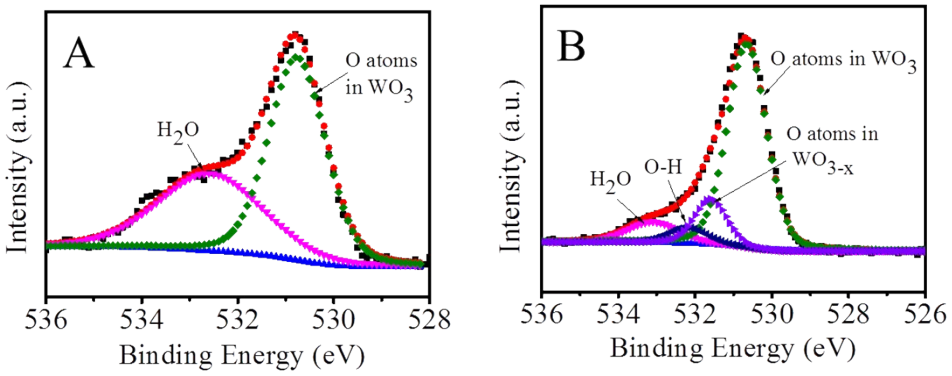

Fig. S8 O1s XPS spectrum for (A) WO_3/NCC and (B)H_xWO_{3-y}/NCC.

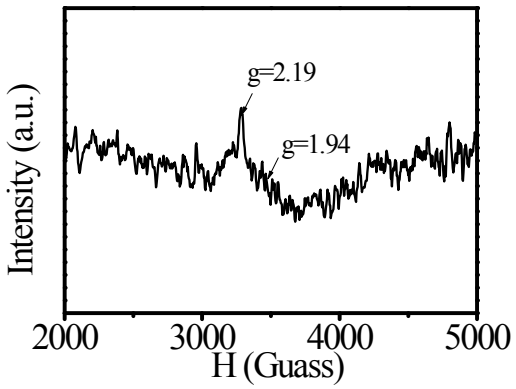

Fig. S9 Electron paramagnetic resonance (EPR) spectrum for H_xWO_{3-y}, where *H* is the magnetic field. The spectrum is collected by subtracting the background of NCC from H_xWO_{3-y}/NCC.

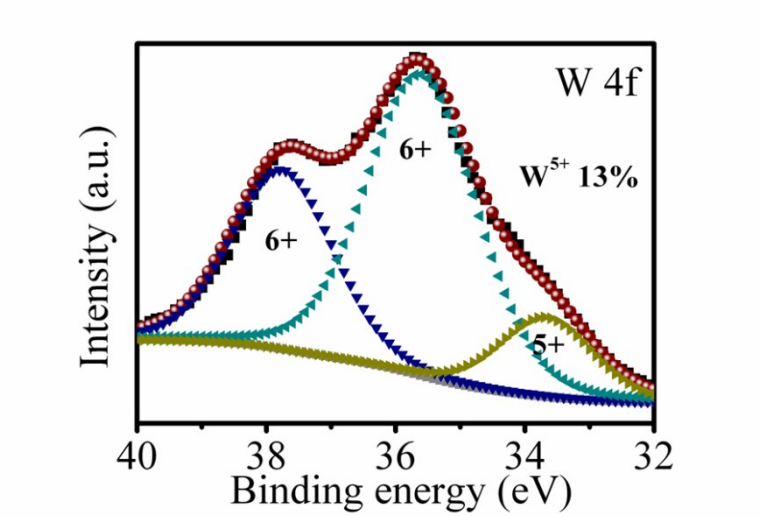

Fig. S10 W 4f XPS spectrum for e-H_xWO_{3-y}/NCC.

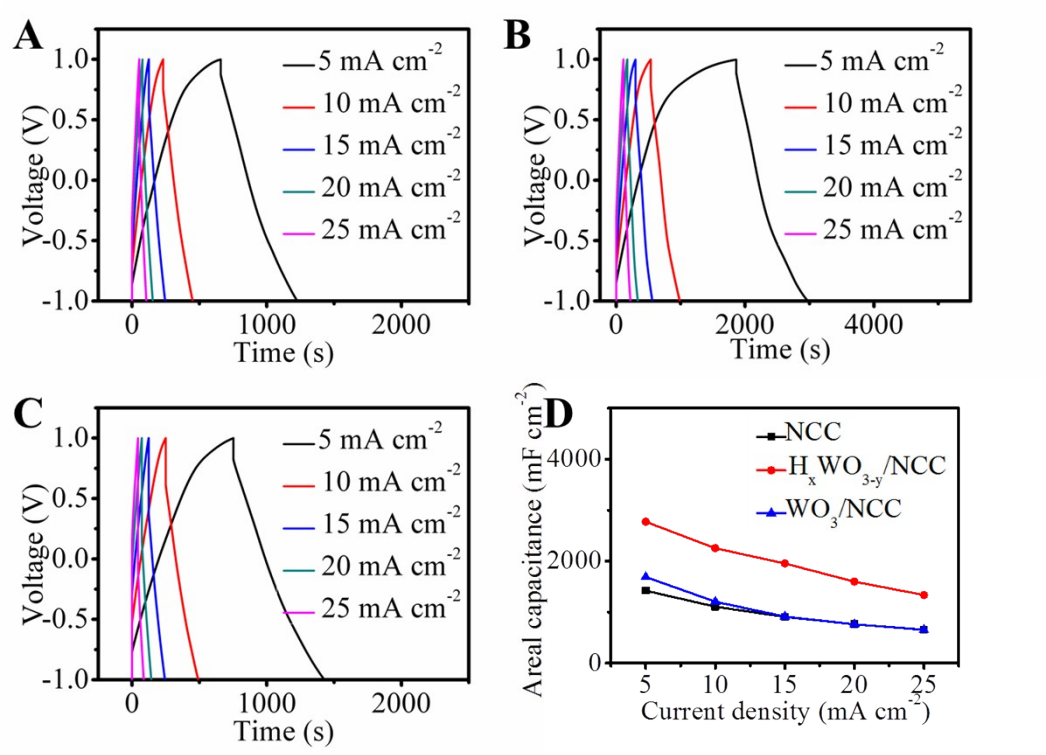

Fig. S11 GCD curves of (A) NCC, (B) H_xWO_{3-y}/NCC and (C) WO_3/NCC at various current densities. (D) The areal capacitances for NCC, H_xWO_{3-y}/NCC and WO_3/NCC based on the GCD curves.

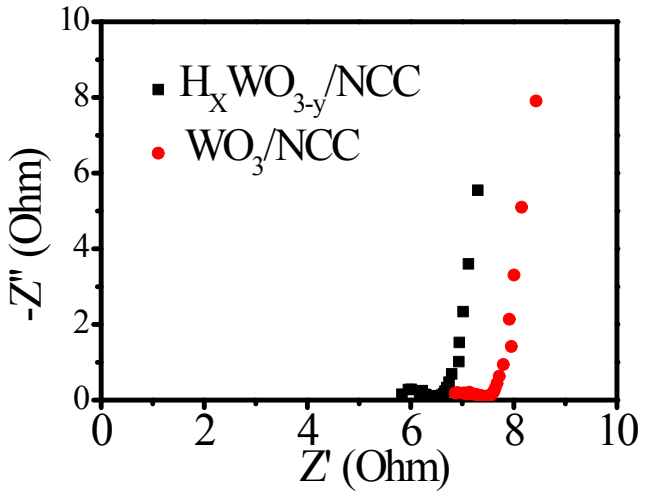

Fig. S12 Nyquist plots for H_xWO_{3-y}/NCC and WO_3/NCC.

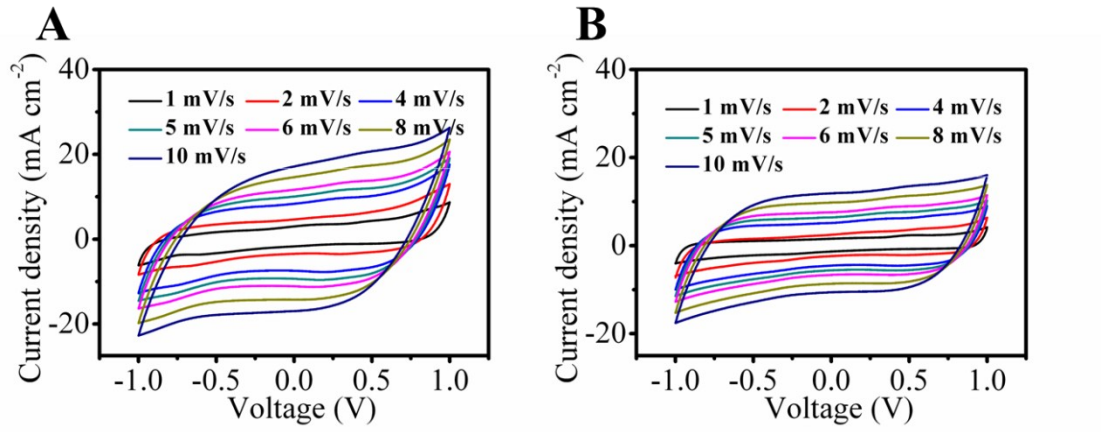

Fig. S13 CV curves of (A) H_xWO_{3-y}/NCC and (B) WO_3/NCC at various sweep rates.

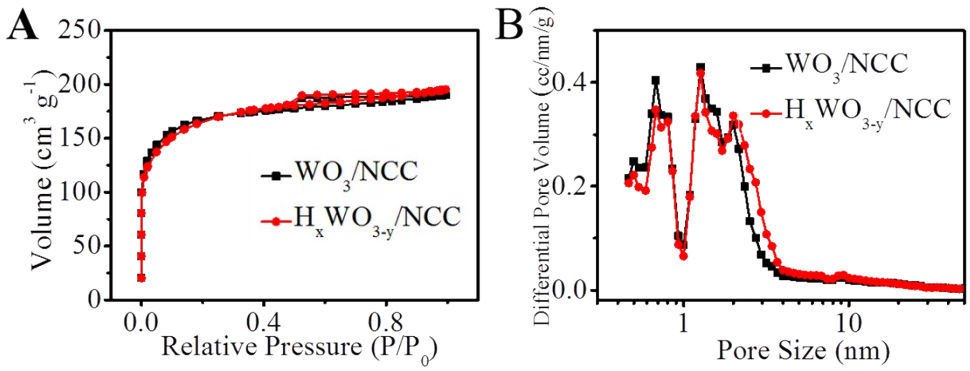

Fig. S14 (A) N_2 adsorption-desorption curves and (B) pore distributions for H_xWO_{3-y}/NCC and WO_3/NCC.

Table S2 Porosity measurements of WO_3/NCC and H_xWO_{3-y}/NCC using nitrogen adsorption/desorption tests.

Materials	S_{BET}[a] ($m^2\ g^{-1}$)	Pore volume ($cm^3\ g^{-1}$)			Average pore width (nm)
		V_{Total}[b]	V_{Micro}[c]	V_{Micro}/V_{Total}	
WO_3/NCC	539	0.293	0.254	0.87	2.18
H_xWO_{3-y}/NCC	544	0.301	0.253	0.85	2.21

[a] Brunuaer–Emmett–Teller surface area; [b] Calculated by single-point adsorption; [c] Calculated by t-plot method.

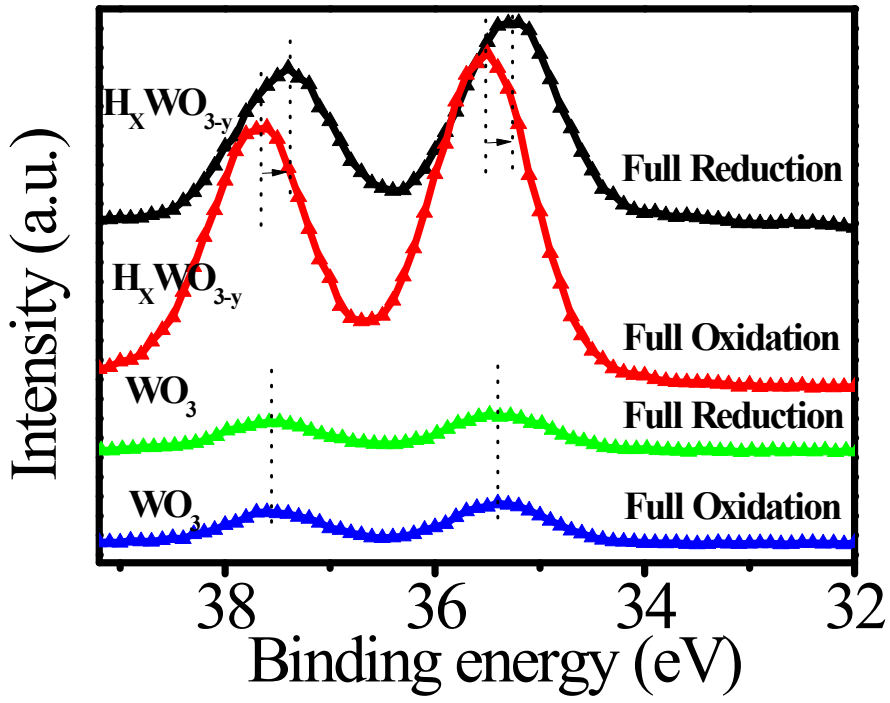

Fig. S15 ex situ XPS spectrum for H_xWO_{3-y} and WO_3 after full reduction and full oxidation.

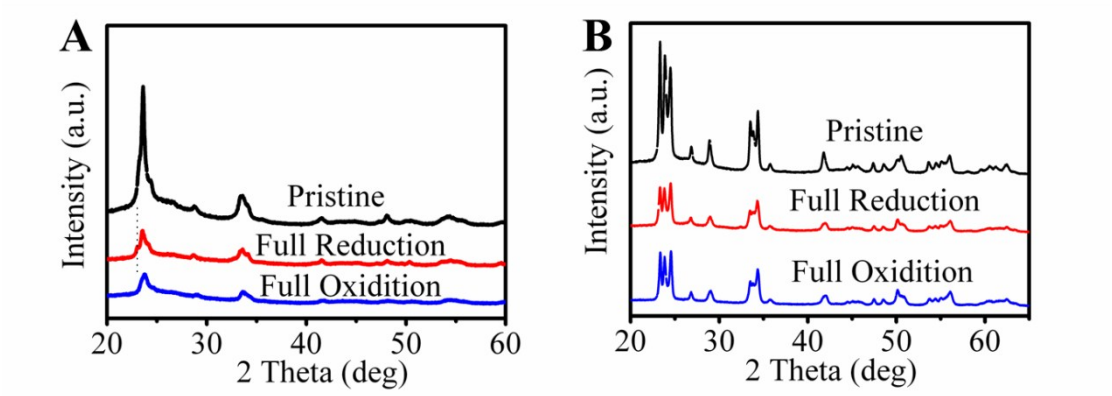

Fig. S16 (A) ex situ XRD patterns for H_xWO_{3-y} and that after full reduction, as well as full oxidation. (B) ex situ XRD patterns for WO_3 and after that full reduction, as well as full oxidation.

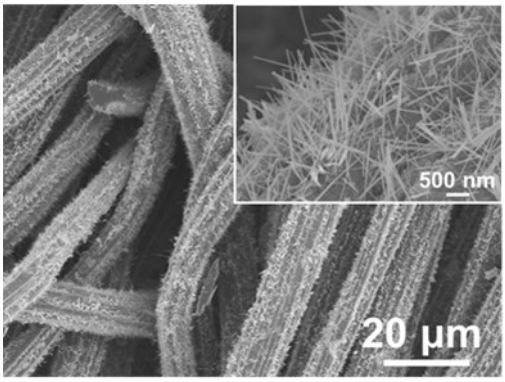

Fig. S17 SEM image of e-H_xWO_{3-y}/NCC.

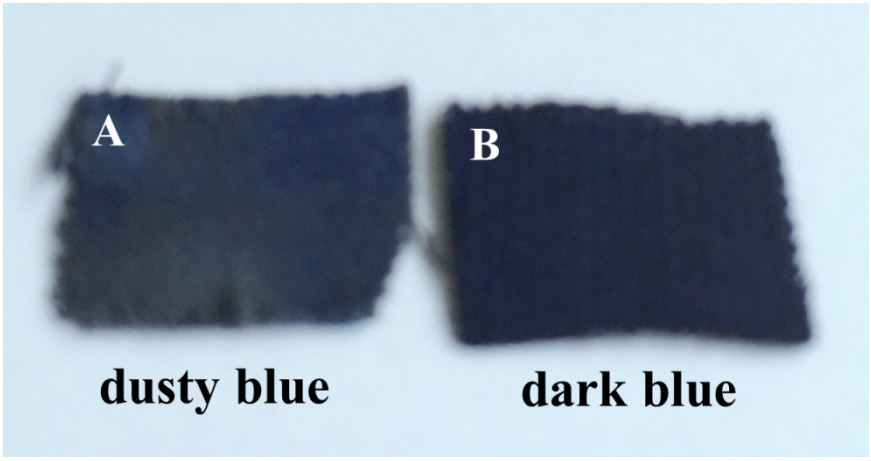

Fig. S18 The digital graph for (A) e-H_XWO_{3-y}/NCC and (B) H_xWO_{3-y}/NCC, showing the color changes from dark blue to dusty blue after argon plasma.

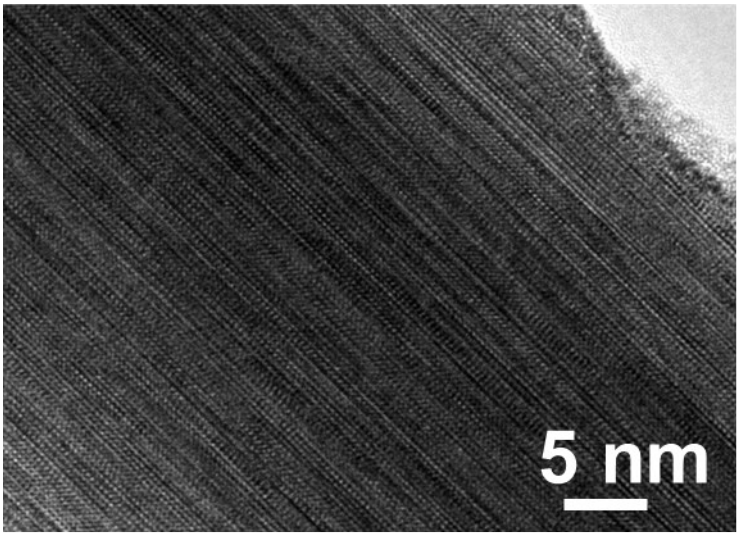

Fig. S19 HRTEM image of e-H_xWO_{3-y}/NCC, suggesting the surface layer of H_xWO_{3-y}/NCC can be etched by argon plasma.

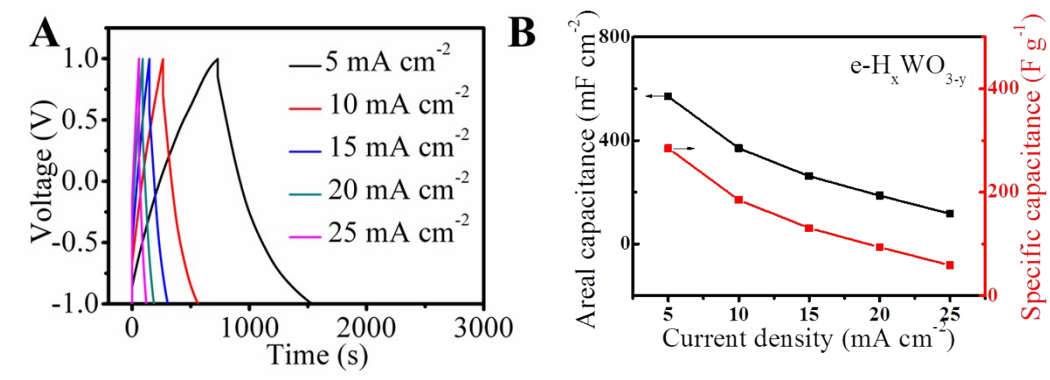

Fig. S20 (A) GCD curves at various current densities for e-H_xWO_{3-y}. (B) The areal capacitances and specific capacitances for e-H_xWO_{3-y}.

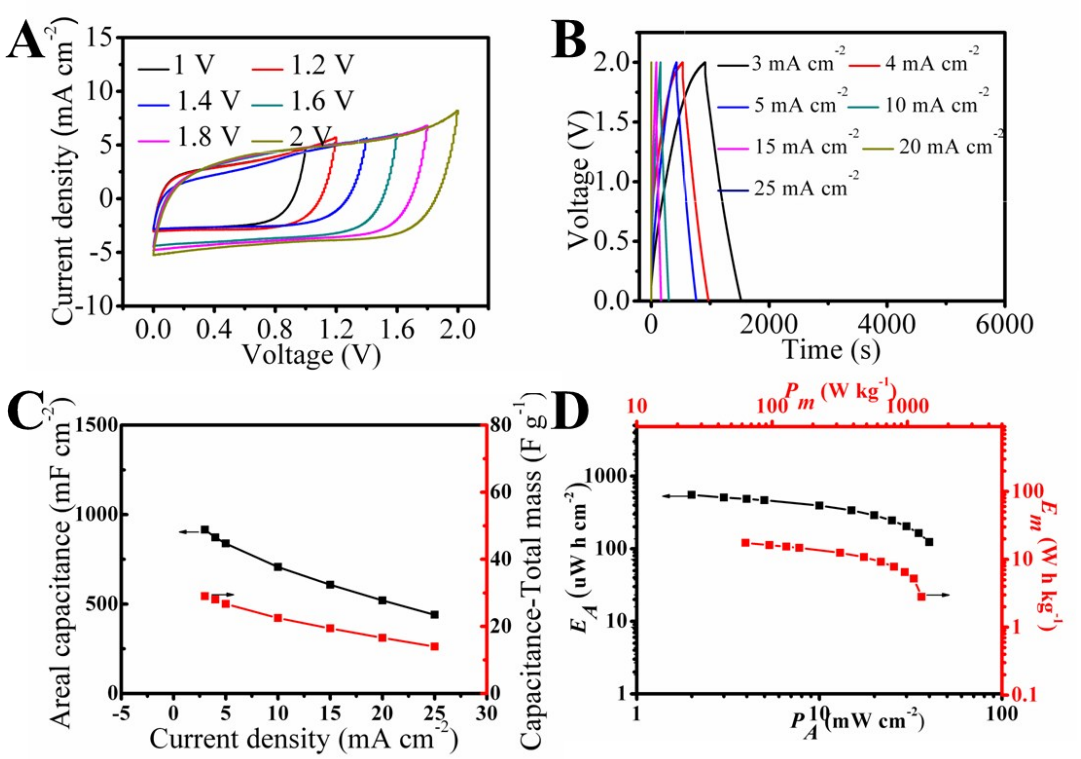

Fig. S21 (A) CV curves for H_xWO_{3-y}/NCC//H_xWO_{3-y}/NCC device, suggesting the voltage window can be extended to 2 V. (b) GCD curves for H_xWO_{3-y}/NCC//H_xWO_{3-y}/NCC device at the current densities range from 3 to 25 mA cm^{-2}. (C) The areal capacitances and gravimetric capaciatances for H_xWO_{3-y}/NCC//H_xWO_{3-y}/NCC based on the total mass of the device. (D) Ragone plot of H_xWO_{3-y}/NCC//H_xWO_{3-y}/NCC device.

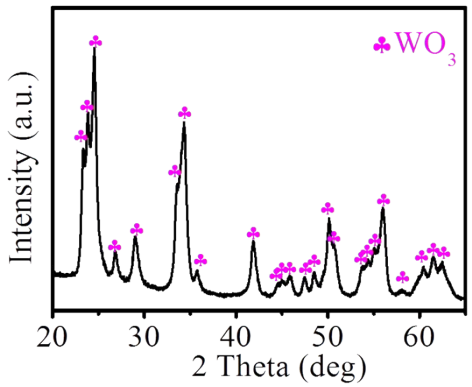

Fig. S22 XRD pattern of the contrast sample synthesized according to the same procedure to H_xWO_{3-y}/NCC but without the intrusion of NCC.

References

1 H. Wang, J. Deng, C. Xu, Y. Chen, F. Xu, J. Wang and Y. Wang, Energy Storage Mater., 2017, **7**, 216.